

pubs.acs.org/JPCB Article

Standalone 2-D Nanosheets and the Consequent Hydrogel and Coacervate Phases Formed by 2.5 nm Spherical U₆₀ Molecular Clusters in Dilute Aqueous Solution

Yuqing Yang, Yifan Zhou, Jiahui Chen, Tsuyoshi Kohlgruber, Travis Smith, Bowen Zheng, Jennifer E. S. Szymanowski, Peter C. Burns,* and Tianbo Liu*



Cite This: J. Phys. Chem. B 2021, 125, 12392-12397



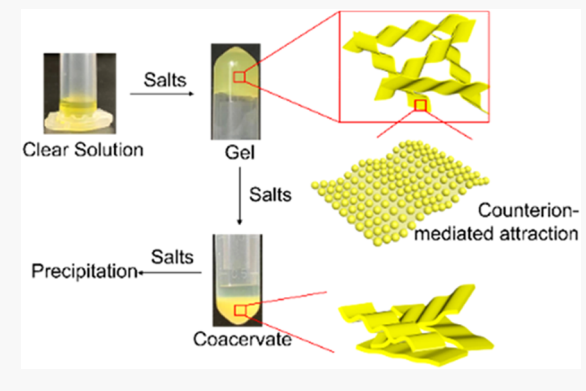
ACCESS

Metrics & More

Article Recommendations

Supporting Information

ABSTRACT: Unexpected hydrogel and coacervate are observed for dilute (1 mM) uranyl peroxide molecular cluster ($\text{Li}_{68}\text{K}_{12}(\text{OH})_{20}[\text{UO}_2(\text{O}_2)-(\text{OH})]_{60}$, U_{60}) solution in the presence of di- or trivalent salts. We report the mechanism as the formation of anisotropic two-dimensional (2-D) single-layer nanosheets, driven by counterion-mediated attraction due to the size disparity between U_{60} and small counterions. With weak monovalent cations, the nanosheets are bendable, resulting in hollow, spherical blackberry-type supramolecular assemblies in a homogeneous solution. With extra strong divalent or trivalent cations, the tough, free-standing sheets lead to gelation at ~ 1 mM U_{60} . These stiff nanosheets are difficult to bend into spherical blackberry-type structures; instead, they stay in solution and form hydrogel based on their significant excluded volumes. At higher ionic strength, the large, thin filmlike nanosheet structures stack



together more compactly and consequently lead to the transition from gel phase to a coacervate phase, another surprise since it was formed without the presence of bulky polycations.

■ INTRODUCTION

Supramolecular two-dimensional (2-D) nanomaterials have garnered extensive attention in recent years for their potential applications in electronics, ^{1,2} catalysis, ³ sensors, ⁴ and drug delivery. ⁵ Despite their promising advantages, much attention has been paid to the synthesis of supramolecular nanosheets whose formation mechanism is yet to be explored.

In dilute aqueous solution, the phase behavior of salts is usually simple, they have certain solubility and phase separation beyond a point if no chemical or coordination interaction occurs. This general understanding may not be accurate for ions with nanoscale size. Such macroions exhibit completely different solution behaviors from small ions and colloidal suspensions⁶ but represent a transition region in between, which cannot be described by either the Debye-Hückel theory for small ions (they are no longer point charges) or the DLVO theory⁸ for colloids (van der Waals forces are negligible for macroions). The size disparity between macroions and their counterions is significant but not dominant, leading to moderate counterion association around macroions in polar solvents and the formation of hollow spherical blackberry structures based on counterion-mediated attraction.6 Through molecular dynamic simulations, clear symmetry breakage happens at the initial stage by charge redistribution closer to the macroion's equatorial area to construct 2-D nanosheets⁹ and consequently blackberry structures.

U₆₀ (Figure 1) is one of the largest members of the uranyl peroxide cluster family with a 2.5 nm diamter and a welldefined C₆₀-like fullerene topology molecular structure, ¹⁰ which consists of 60 uranyl polyhedra. Its 60- charge and hydrophilic surface (hydration layer) make it highly soluble in aqueous solutions, while the overall structure remains intact for months. 11 Due to its high charge density, U₆₀ stays as discrete macroions in a dilute aqueous solution with high solubility¹² and tends to self-assemble into hollow, spherical, single-layered blackberry structure in the presence of additional monovalent counterions, e.g., K⁺. ¹³ Here, two unexpected new phases, hydrogel and coacervate, are discovered in the dilute U₆₀ aqueous solutions with the addition of di-/trivalent counterions. Without the assistance of any common driving force for gelation, e.g., hydrophobic, $\pi - \pi$, host–guest interaction, or the presence of bulky polycations, it is unlikely to observe hydrogel

Revised: September 10, 2021 Revised: October 14, 2021 Published: October 27, 2021





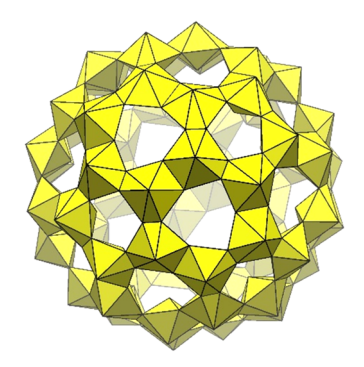


Figure 1. Polyhedral representation of U_{60} . The $[(UO_2)(O_2)_2(OH)_2]$ subunits of 2.5 nm diameter U_{60} are represented by yellow hexagonal bipyramids.

and coacervation in dilute solutions only containing U_{60} and small electrolytes.

METHODS

Gel and Coacervate Preparation. Solid samples of the U_{60} cluster were dissolved directly in water to obtain a concentrated solution that was diluted to appropriate concentrations for characterization. All of the solutions were dust-free after passing through poly(tetrafluoroethylene) (PTFE) filters. Concentrated salt aqueous solutions or solid salts (to avoid the excess dilution of U_{60} at a high salt/ U_{60} ratio) were added to U_{60} aqueous solutions and an inversion test was conducted after 5 min standing after each addition.

At an appropriate concentration, the U_{60} aqueous solution (1.0-4.0 mM for U₆₀ solution with YCl₃ and 1.0-6.0 mM for U₆₀ solution with BaCl₂ or SrCl₂) remains clear yellow liquid with the addition of small amounts of salts. As further salt solutions are added, a clear gel is observed that does not flow when the tube is turned upside-down. With large amounts of salts, coacervate that shows a clear liquid-liquid phase separation with a yellow bottom part and a colorless top part is obtained. Also, a small volume increase of the colorless top part is noticed with an elevated amount of added SrCl₂. Finally, a powder-like precipitate can be seen when excess SrCl₂ is introduced. For dilute or concentrated U_{60} aqueous solution (<1.0 mM and >6.0 mM for U₆₀ solution with BaCl₂ or SrCl₂ or <1.0 mM and >4.0 mM for U₆₀ solution with YCl₃), a transition from a homogeneous yellow solution to a liquidliquid-separated coacervate was observed with the addition of salts with no gel obtained.

Small-Amplitude Oscillatory Shear (SAOS). The SAOS studies were performed using 15.367 mm parallel plates geometry on a Physica MCR-301 rheometer from AntonPaar. The measurements were done at room temperature in air. The strain changed logarithmically from 0.01 to 10%, with five points recorded per decade, and the angular frequency was fixed at 10 rad/s.

Transmission Electron Microscopy (TEM). A small amount of solution dropped onto a holey carbon film placed on a copper grid was dried and used to take images with a JEOLJEM-1230 electron microscope operated at 120 kV.

Isothermal Titration Calorimetry (ITC). ITC measurements were performed using a standard volume Nano ITC isothermal titration calorimeter (TA Instruments) with 1.0 mL

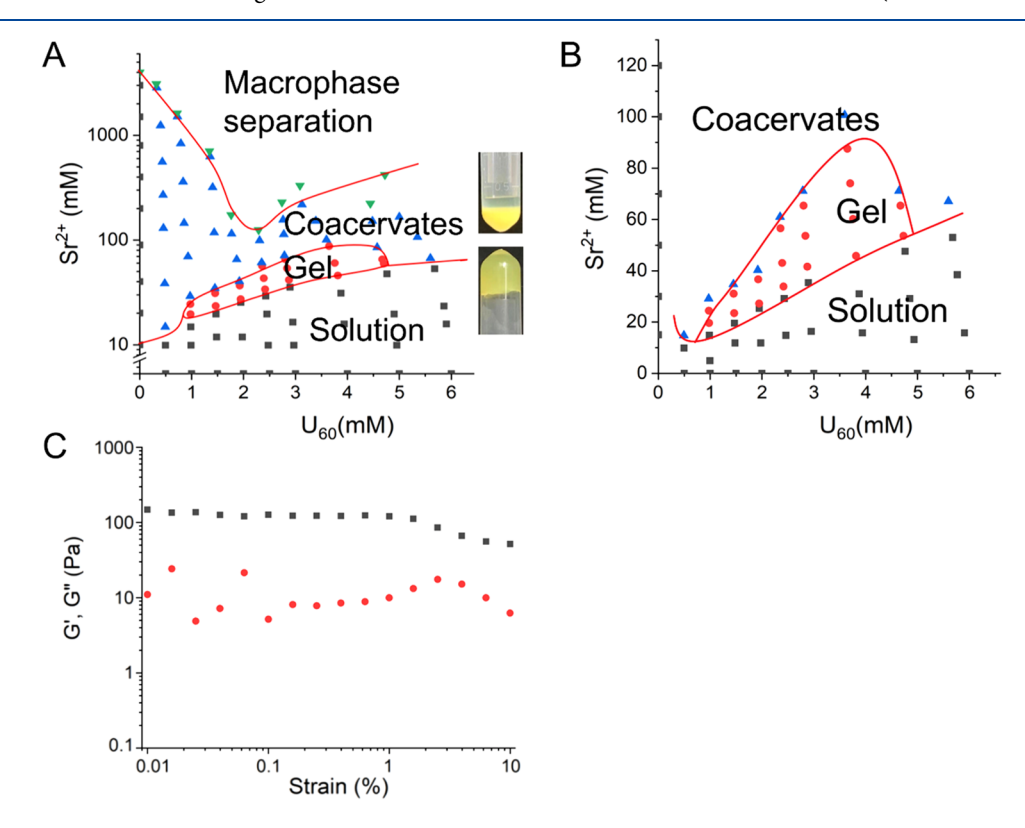


Figure 2. (A, B) U_{60} -SrCl₂ binary phase diagram in dilute aqueous solution. Solution (black squares), gel (red circles), coacervate (blue triangles), and macrophase separation (green inverted triangles) phases with approximate boundaries are shown with photos of the coacervate (right up) and gel (right down). (C) Rheology study of the U_{60} gel. The storage modulus (G', black) and loss modulus (G'', red) of 1 mM U_{60} gel samples with 20 mM SrCl₂ at 300 K.

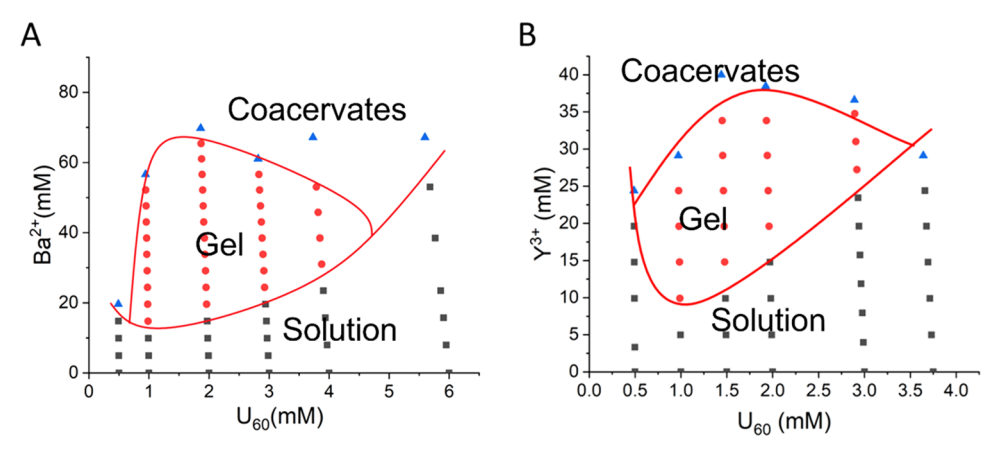
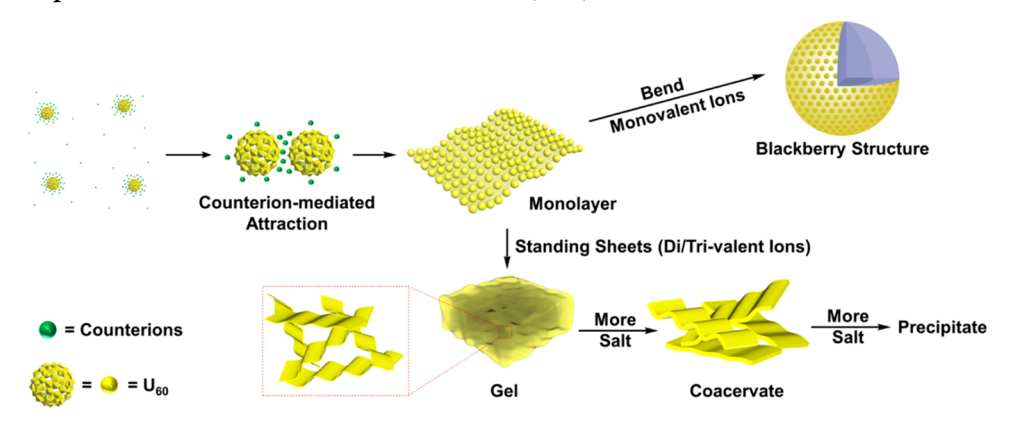


Figure 3. Simplified aqueous U_{60} clusters—BaCl₂/YCl₃ binary phase diagram. Solution (black squares), gel (red circles), and coacervate (blue triangles) phases with approximate boundaries are shown for (A) U_{60}/Ba^{2+} system and (B) U_{60}/Y^{3+} system.

Scheme 1. U₆₀ in Aqueous Solution with the Addition of Mono-, Di-, or Trivalent Counterions^a



"Counterion-mediated attraction promotes the formation of U_{60} nanosheets. Flexible U_{60} nanosheets formed with monovalent counterions bend to form blackberry structures; di-/trivalent counterions and U_{60} lead to more rigid, standalone nanosheets and then hydrogel and coacervate.

of Hastelloy C sample cell and 250 μ L syringe. The experiments were carried out at 25 °C using 25 consecutive injections of 10 μ L. A rotation rate of 250 rpm was used to ensure the proper, continuous mixing of solutions in the chamber. In all experiments, the background heat was subtracted to reach the final results. The independent binding site model was applied to analyze the results, which provided the binding number and interaction energy between U_{60} clusters and different salts.

High-Resolution Scanning Electron Microscopy (HRSEM). Morphological analyses of the samples were performed using a high-resolution scanning electron microscope (HRSEM) type Tescan Lyra 3 XMU at the operating voltage of 20 kV and a JEOL JCM-6000PLUS NeoScope Benchtop SEM using a secondary electron detector (SED) with an accelerating voltage of 5–10 kV. The samples were freeze-dried before imaging.

■ RESULTS AND CONCLUSIONS

Gelation of U₆₀. Upon introducing 20 mM $SrCl_2$ into a 1.0 mM (~20 mg/mL) U₆₀ solution, the original dilute solution transforms to a homogeneous, transparent gel phase. The phase diagram (Figure 2A) indicates that the gel phase covers a considerable area, ranging from 1 to 5 mM U₆₀ and 20 to 80 mM Sr^{2+} . Rheological studies (Figure 2C) reveal their gel state, as the storage modulus (G') is higher than the loss modulus

(G'') within a certain range of strain. The relatively small values of G' and G'', compared with the polymer gel, are a typical feature of a weak hydrogel, likely based on electrostatic interactions.

Upon further increasing the Sr²⁺ concentration, the U₆₀ gels demonstrate an obvious transition to two separate, stable liquid phases, with the upper layer being clear and colorless, containing no U₆₀, while the lower layer is in yellow color (Figure 2A). This is a typical coacervate phase.¹⁴ The coacervate region covers a large area in the phase diagram (Figure 2A). At very high Sr²⁺ concentrations, considerable amounts of solid precipitates accumulate at the bottom of the lower liquid phase, indicating that U₆₀ has separated from the solution due to its limited solubility. The roughly U-shaped phase separation curve with U₆₀ concentration in the phase diagram is similar to that of hydrophilic polymers in aqueous solution; 15 the enhanced screening effect from the extra salts decreases the solubility of U₆₀ macroions. Similar gel and coacervate phases were also identified in U_{60}/Y^{3+} and $\tilde{U_{60}}/Ba^{2+}$ solutions (Figure 3).

Critical Gelation Conditions. It is observed that with different cations, the lowest gelation concentration for U_{60} is always ~ 1.0 mM, while the highest U_{60} concentration for the gel region is ~ 5 mM with divalent cations and ~ 3 mM with trivalent cations.

For other boundary conditions, the sol-to-gel transition curve roughly follows the trend of molar ratio $Y^{3+}/U_{60}^{-}=$

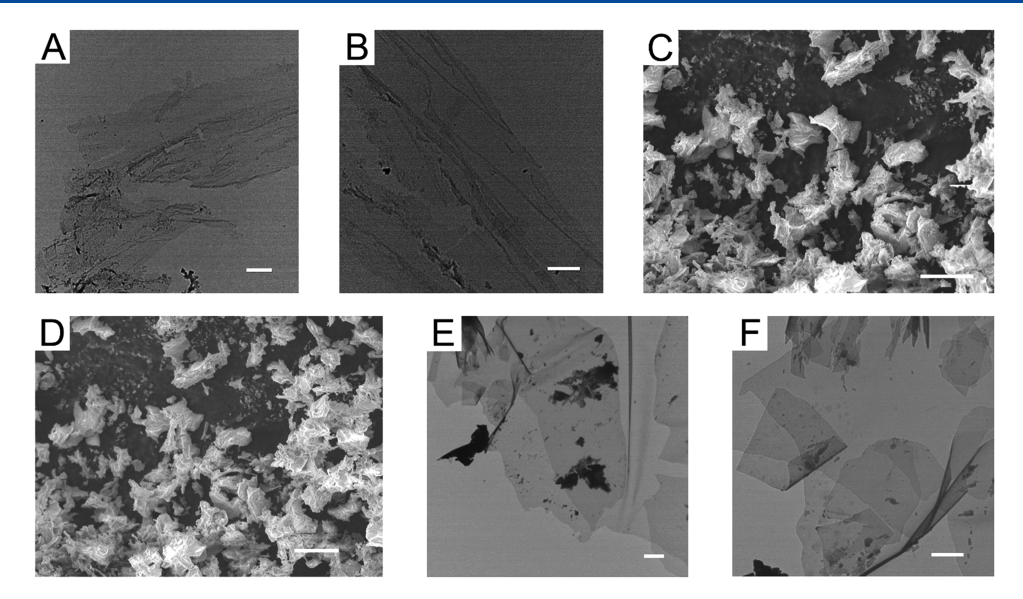


Figure 4. TEM and SEM images of U_{60} with SrCl₂. TEM images of (A, B) 1.0 mM U_{60} solution with 10 mM SrCl₂ or (E, F) 0.5 mM U_{60} with 2 M SrCl₂. (C, D) SEM images of 2.5 mM U_{60} gel with 30 mM SrCl₂. Scale bar: (A) 1 μ m, (B) 800 nm, (C) 20 μ m, (D) 20 μ m, (E) 2 μ m, and (F) 800 nm.

10:1, or a total charge ratio of 30:60, for different U_{60} concentrations. This critical ratio is the quantity of Y^{3+} ions needed to generate enough nanosheet structures in solution for gel formation. Similar phenomena were observed with Sr^{2+} or Ba^{2+} , but with higher critical molar ratios (for Sr^{2+} : \sim 20:1; Ba^{2+} : \sim 15:1) at 1.0 mM U_{60} concentration with charge ratios of 40:60 and 30:60, respectively. The affinity of Ba^{2+} ions with the U_{60} cluster is comparatively stronger than that of Sr^{2+} , which is also confirmed by the isothermal titration calorimetry (ITC) data, the Ba^{2+} – U_{60} interaction releases more heat under the same conditions in comparison to Sr^{2+} (Figure S2). Different from Y^{3+} , for divalent cations, the sol—gel transition curves show lower slopes: the critical molar ratios gradually drop to \sim 13:1 for Sr^{2+} and <10:1 for Ba^{2+} with increasing U_{60} concentration.

Mechanism of Gelation. The gelation of small molecules requires them to be assembled into anisotropic and open supramolecular structures so that large excluded volumes increase the lifetime of interparticle bonds to make them able to sustain stress, surviving for longer than the experimental probe characteristic time, ¹⁶ in which case leading to the observed gelation. Such open structures can be formed via chemical cross-linking (rubbers¹⁷), metal coordination, ¹⁸ or physical interactions such as hydrogen bond, ¹⁹ $\pi - \pi$ interaction, ²⁰ hydrophobic interaction (surfactant gels), ²¹ van der Waals forces (colloid gels), ²² host—guest interaction, ²³ or chain entanglement (polymer gels), ²⁴ among which, electrostatic interaction is not the common driving force. None of the above-mentioned gelation mechanisms are applicable to U₆₀ due to the lack of corresponding intermolecular forces. That is, we are dealing with a new type of gel whose formation might be related to their unique feature as macroions.

As shown in Scheme 1, the counterion-mediated attraction has been experimentally observed and confirmed by simulations in macroionic systems 25 including U_{60} , leading to the formation of 2-D single-layer sheets. Often such sheets grow and close to form hollow, single-layer, blackberry-type structures in polar solvents; this is also the case when Li⁺/Na⁺ are the counterions and blackberry structures are formed;

in the meantime, the solution remained clear and homogeneous.⁸ Stronger counterions (higher valence and/or smaller hydrated size) result in stronger counterion-mediated attraction among macroions and slightly shorter inter-macroionic distance, resulting in more rigid sheets and larger blackberry structures (more difficult for the sheets to bend).²⁶ If the nanosheets are too tough to bend, they could stay as sheets in solution. High-resolution TEM images (Figures 4A,B and S1A-C) confirm that many large-scale, open structures have formed in 1.0 mM U₆₀ aqueous solution with 10 mM SrCl₂ (still a mobile solution to avoid severe aggregation on the TEM grid). With increasing SrCl₂, scanning electron microscopy (SEM) (Figures 4C,D and S1D,E) images of freeze-dried samples contained abundant open nanosheets from the system; meanwhile, the solution of U₆₀ turns into a gel. The transparency of the sheets under the TEM clearly demonstrated their very thin nature. They can grow into several microns in size, providing significant excluded volumes which hinder their diffusion and lead to gelation. Recently, another case of electrostatic-interaction-based gelation was reported for a cationic metal-organic cage.²⁷ With extra salts, counterion-mediated attraction between cages, along with other types of interactions (π – π , σ - π and hydrophobic), leads to the formation of stiff nanosheets and then gelation. U₆₀ represents a much better model system in which electrostatic interaction is the sole source of attraction.

ITC measurements (Figure S2) quantitatively show the U_{60} -cation interaction. The sudden change of heat release from U_{60} and $\mathrm{Sr^{2+}/Ba^{2+}/Y^{3+}}$ systems indicates the occurrence of the complex interactions when di- or trivalent cations are introduced into the U_{60} solution. Meanwhile, the large heat release suggests much stronger U_{60} -counterion interactions for di- and trivalent cations, in comparison with that of monovalent counterions.

At a given composition, the sol–gel transition can be achieved by increasing the temperature. A higher temperature promotes the mobility of ions 6 and decreases the stability of the supramolecular nanosheets, making the gels less stable. An example (Figure S3) is the gel of 1.0 mM U_{60} with 10 mM

YCl₃. The clear gel transits to a clear solution at 70 $^{\circ}$ C; and the gel forms again when the temperature drops. The process is reversible and reproducible for multiple cycles.

Gel-to-Coacervate Transition. Coacervate is a liquidliquid separation with a dilute supernatant and a dense macromolecule-rich phase that is driven by electrostatic attraction between oppositely charged macroions, 8 usually polyelectrolytes. Many charged macromolecules, e.g., colloids, ²⁸ proteins, ²⁹ or polymers, ³⁰ are observed to be involved in coacervation processes. Among these species, a stronger tendency for coacervate formation is found when components contain longer chains.³¹ Its formation becomes less likely if the two components show a disparity in charge numbers. Here, coacervates are observed when $U_{60}^{\,\,60-}$ anions are mixed with small divalent or trivalent cations, which is unexpected from the perspective of traditional coacervates. This coacervate phase appears above the gel phase in the phase diagram, i.e., at higher ionic strength. TEM studies (Figures 4E,F and S4) on the coacervates show large, thin-film-like nanosheet structures similar to those observed in the gel phase. Meanwhile, the stacking of nanosheets seems to be more compact. This could be explained as excess amounts of salts further strengthen the attraction among the nanosheets and bring them closer, leading to the apparent liquid-liquid phase separation.

The coacervate area covers a significant range of salt concentrations, showing that this metastable phase is dominant (or it takes a very long time for them to further phase separate, beyond the time frame of experiments). At very high salt concentrations, considerable solid precipitates are observed at the bottom of containers, indicating that the $\rm U_{60}$ clusters are not soluble anymore due to the enhanced screening effect.

CONCLUSIONS

In summary, nanoscale macroions demonstrate complicated phase behaviors even in their dilute solutions. The imbalance between macroions and small counterions leads to counterion association and then counterion-mediated attraction among macroions, causing them to assemble into 2-D nanosheet structures. With weaker counterions, the nanosheets further bend and enclose to form hollow, spherical blackberry-type structures; with stronger counterions, the rigid nanosheets stand along in dilute aqueous solution, leading to large extended volumes and consequent gelation. With increasing ionic strength, such electrostatic-based gels further collapse into the coacervate phase due to the closer stacking of nanosheets. Eventually, U60 macroions precipitate from the solution at very high ionic strength. The newly discovered gel and coacervate phases are expected to be general for macroions and open new opportunities for nanoscale materials with counterion-mediated attraction as the driving force.

ASSOCIATED CONTENT

Supporting Information

The Supporting Information is available free of charge at https://pubs.acs.org/doi/10.1021/acs.jpcb.1c08019.

Detailed sample preparation methods, SAOS, TEM, SEM, and ITC data (PDF)

(PDF)

AUTHOR INFORMATION

Corresponding Authors

Peter C. Burns — Department of Civil Engineering and Geological Sciences, University of Notre Dame, Notre Dame, Indiana 46556, United States; orcid.org/0000-0002-2319-9628; Email: pburns@nd.edu

Tianbo Liu — School of Polymer Science and Polymer Engineering, The University of Akron, Akron, Ohio 44325, United States; ⊙ orcid.org/0000-0002-8181-1790; Email: tliu@uakron.edu

Authors

Yuqing Yang — School of Polymer Science and Polymer Engineering, The University of Akron, Akron, Ohio 44325, United States; orcid.org/0000-0002-5407-5740

Yifan Zhou — School of Polymer Science and Polymer Engineering, The University of Akron, Akron, Ohio 44325, United States

Jiahui Chen – School of Polymer Science and Polymer Engineering, The University of Akron, Akron, Ohio 44325, United States

Tsuyoshi Kohlgruber – Department of Civil Engineering and Geological Sciences, University of Notre Dame, Notre Dame, Indiana 46556, United States

Travis Smith — School of Polymer Science and Polymer Engineering, The University of Akron, Akron, Ohio 44325, United States

Bowen Zheng - Copley High School, Akron, Ohio 44321, United States

Jennifer E. S. Szymanowski — Department of Civil Engineering and Geological Sciences, University of Notre Dame, Notre Dame, Indiana 46556, United States

Complete contact information is available at: https://pubs.acs.org/10.1021/acs.jpcb.1c08019

Author Contributions

Y.Y., Y.Z., J.C., P.C.B., and T.L. conceptualized and designed the study; T.K. and J.E.S.S. synthesized the sample; T.S. did the SAOS measurements; T.K., Y.Y., and Y.Z. did TEM and SEM measurements; Y.Y. and Y.Z. collected and analyzed the data; Y.Y., Y.Z., and T.L. edited the manuscript.

Funding

The National Science Foundation (NSF CHE1904397) and the National Nuclear Security Administration, Department of Energy, under Award No. DE-Na0003763A.

Notes

The authors declare no competing financial interest.

ACKNOWLEDGMENTS

T.L. acknowledges support from the National Science Foundation (NSF CHE1904397) and the University of Akron. P.C.B. acknowledges support from the National Nuclear Security Administration, Department of Energy, under Award No. DE-Na0003763, and the University of Notre Dame.

REFERENCES

- (1) Hu, B.; Sun, S.; Wu, B.; Wu, P. Colloidally Stable Monolayer Nanosheets with Colorimetric Responses. *Small* **2019**, *15*, No. 1804975.
- (2) Butler, S. Z.; Hollen, S. M.; Cao, L.; Cui, Y.; Gupta, J. A.; Gutiérrez, H. R.; Heinz, T. F.; Hong, S. S.; Huang, J.; Ismach, A. F.;

- et al. Progress, Challenges, and Opportunities in Two-Dimensional Materials Beyond Graphene. ACS Nano 2013, 7, 2898–2926.
- (3) Lin, Y.; Thomas, M. R.; Gelmi, A.; Leonardo, V.; Pashuck, E. T.; Maynard, S. A.; Wang, Y.; Stevens, M. M. Self-Assembled 2D Free-Standing Janus Nanosheets with Single-Layer Thickness. *J. Am. Chem. Soc.* 2017, 139, 13592–13595.
- (4) Liu, Y.; Jiao, Y.; Zhang, Z.; Qu, F.; Umar, A.; Wu, X. Hierarchical SnO2 Nanostructures Made of Intermingled Ultrathin Nanosheets for Environmental Remediation, Smart Gas Sensor, and Supercapacitor Applications. ACS Appl. Mater. Interfaces 2014, 6, 2174–2184.
- (5) Zhang, T.; Zhang, C.-H. Photo-controlled reversible secondary self-assembly of supramolecular nanosheets and their drug delivery behavior. *J. Mater. Chem. B* **2019**, *7*, 7736–7743.
- (6) Liu, T. Hydrophilic Macroionic Solutions: What Happens When Soluble Ions Reach the Size of Nanometer Scale? *Langmuir* **2010**, 26, 9202–9213.
- (7) Debye, P.; Hückel, E. De la theorie des electrolytes. I. abaissement du point de congelation et phenomenes associes. *Phys. Z.* **1923**, 24, 185–206.
- (8) Russel, W. B.; Russel, W.; Saville, D. A.; Schowalter, W. R. Colloidal Dispersions; Cambridge University Press, 1991.
- (9) Liu, Z.; Liu, T.; Tsige, M. Unique Symmetry-Breaking Phenomenon during the Self-assembly of Macroions Elucidated by Simulation. *Sci. Rep.* **2018**, *8*, No. 13076.
- (10) Sigmon, G. E.; Unruh, D. K.; Ling, J.; Weaver, B.; Ward, M.; Pressprich, L.; Simonetti, A.; Burns, P. C. Symmetry versus Minimal Pentagonal Adjacencies in Uranium-Based Polyoxometalate Fullerene Topologies. *Angew. Chem., Int. Ed.* **2009**, *48*, 2737–2740.
- (11) Peruski, K. M.; Bernales, V.; Dembowski, M.; Lobeck, H. L.; Pellegrini, K. L.; Sigmon, G. E.; Hickam, S.; Wallace, C. M.; Szymanowski, J. E. S.; Balboni, E.; et al. Uranyl Peroxide Cage Cluster Solubility in Water and the Role of the Electrical Double Layer. *Inorg. Chem.* 2017, 56, 1333–1339.
- (12) Gao, Y.; Szymanowski, J. E. S.; Sun, X.; Burns, P. C.; Liu, T. Thermal Responsive Ion Selectivity of Uranyl Peroxide Nanocages: An Inorganic Mimic of K+ Ion Channels. *Angew. Chem., Int. Ed.* **2016**, 55, 6887–6891.
- (13) Gao, Y.; Haso, F.; Szymanowski, J. E. S.; Zhou, J.; Hu, L.; Burns, P. C.; Liu, T. Selective Permeability of Uranyl Peroxide Nanocages to Different Alkali Ions: Influences from Surface Pores and Hydration Shells. *Chem. Eur. J.* **2015**, *21*, 18785–18790.
- (14) Sing, C. E.; Perry, S. L. Recent progress in the science of complex coacervation. *Soft Matter* **2020**, *16*, 2885–2914.
- (15) Johansson, H.-O.; Feitosa, E.; Junior, A. P. Phase Diagrams of the Aqueous Two-Phase Systems of Poly(ethylene glycol)/Sodium Polyacrylate/Salts. *Polymers* **2011**, *3*, 587–601.
- (16) Deng, N.-J.; Luo, Y.-Z.; Tanodekaew, S.; Bingham, N.; Attwood, D.; Booth, C. Gelation of micellar solutions of diblock-copoly (oxyethylene/oxybutylene) in aqueous K2SO4. An investigation of excluded volume effects. *J. Polym. Sci., Part B: Polym. Phys.* 1995, 33, 1085–1096.
- (17) Zhao, J.; Yang, R.; Iervolino, R.; Barbera, S. Investigation of crosslinking in the thermooxidative aging of nitrile—butadiene rubber. *J. Appl. Polym. Sci.* **2015**, *132*, No. 41319.
- (18) Fages, F. Metal Coordination To Assist Molecular Gelation. *Angew. Chem., Int. Ed.* **2006**, 45, 1680–1682.
- (19) Stanley, H. E.; Blumberg, R. L.; Geiger, A. Gelation models of hydrogen bond networks in liquid water. *Phys. Rev. B* **1983**, 28, 1626–1629.
- (20) Zhang, Y.-M.; Zhu, W.; Qu, W.-J.; Zhong, K.-P.; Chen, X.-P.; Yao, H.; Wei, T.-B.; Lin, Q. Competition of cation— π and exo-wall π — π interactions: a novel approach to achieve ultrasensitive response. *Chem. Commun.* **2018**, *54*, 4549—4552.
- (21) Hussain, H.; Tan, B. H.; Seah, G. L.; Liu, Y.; He, C. B.; Davis, T. P. Micelle Formation and Gelation of (PEG–P(MA-POSS)) Amphiphilic Block Copolymers via Associative Hydrophobic Effects. *Langmuir* **2010**, *26*, 11763–11773.

- (22) Lattuada, M.; Wu, H.; Morbidelli, M. Experimental Investigation of Colloidal Gel Structures. *Langmuir* **2004**, *20*, 4355–4362.
- (23) Zhang, M.; Xu, D.; Yan, X.; Chen, J.; Dong, S.; Zheng, B.; Huang, F. Self-Healing Supramolecular Gels Formed by Crown Ether Based Host–Guest Interactions. *Angew. Chem., Int. Ed.* **2012**, *51*, 7011–7015.
- (24) Nayak, A. K.; Das, B. Introduction to Polymeric Gels. In *Polymeric Gels*; Pal, K.; Banerjee, I., Eds.; Woodhead Publishing, 2018; Chapter 1, pp 3–27.
- (25) Liu, Z.; Liu, T.; Tsige, M. Elucidating the Origin of the Attractive Force among Hydrophilic Macroions. *Sci. Rep.* **2016**, *6*, No. 26595.
- (26) Pigga, J. M.; Teprovich, J. A.; Flowers, R. A.; Antonio, M. R.; Liu, T. Selective Monovalent Cation Association and Exchange around Keplerate Polyoxometalate Macroanions in Dilute Aqueous Solutions. *Langmuir* **2010**, *26*, 9449–9456.
- (27) Yang, Y.; Rehak, P.; Xie, T.-Z.; Feng, Y.; Sun, X.; Chen, J.; Li, H.; Král, P.; Liu, T. Nanosheets and Hydrogels Formed by 2 nm Metal—Organic Cages with Electrostatic Interaction. *ACS Appl. Mater. Interfaces* **2020**, *12*, 56310–56318.
- (28) Furlani, F.; Sacco, P.; Marsich, E.; Donati, I.; Paoletti, S. Highly monodisperse colloidal coacervates based on a bioactive lactose-modified chitosan: From synthesis to characterization. *Carbohydr. Polym.* **2017**, *174*, 360–368.
- (29) Hwang, D. S.; Zeng, H.; Srivastava, A.; Krogstad, D. V.; Tirrell, M.; Israelachvili, J. N.; Waite, J. H. Viscosity and interfacial properties in a mussel-inspired adhesive coacervate. *Soft Matter* **2010**, *6*, 3232–3236.
- (30) Li, L.; Srivastava, S.; Andreev, M.; Marciel, A. B.; de Pablo, J. J.; Tirrell, M. V. Phase Behavior and Salt Partitioning in Polyelectrolyte Complex Coacervates. *Macromolecules* **2018**, *51*, 2988–2995.
- (31) Spruijt, E.; Westphal, A. H.; Borst, J. W.; Cohen Stuart, M. A.; van der Gucht, J. Binodal Compositions of Polyelectrolyte Complexes. *Macromolecules* **2010**, *43*, 6476–6484.